

Evidence of spin-phonon coupling in CrSiTe₃A. Milosavljević,¹ A. Šolajić,¹ J. Pešić,¹ Yu Liu (刘育),² C. Petrovic,² N. Lazarević,^{1,*} and Z. V. Popović^{1,3}¹*Center for Solid State Physics and New Materials, Institute of Physics Belgrade, University of Belgrade, Pregrevica 118, 11080 Belgrade, Serbia*²*Condensed Matter Physics and Materials Science Department, Brookhaven National Laboratory, Upton, New York 11973-5000, USA*³*Serbian Academy of Sciences and Arts, Knez Mihailova 35, 11000 Belgrade, Serbia*

(Received 12 July 2018; published 18 September 2018; corrected 28 March 2019)

We present Raman scattering results on the layered semiconducting ferromagnetic compound CrSiTe₃. Four Raman-active modes, predicted by symmetry, are observed and assigned. The experimental results are supported by density functional theory calculations. The self-energies of the A_g^3 and the E_g^3 symmetry modes exhibit unconventional temperature evolution around 180 K. In addition, the doubly degenerate E_g^3 mode shows a clear change of asymmetry in the same temperature region. The observed behavior is consistent with the presence of the previously reported short-range magnetic order and strong spin-phonon coupling.

DOI: [10.1103/PhysRevB.98.104306](https://doi.org/10.1103/PhysRevB.98.104306)**I. INTRODUCTION**

Trichalcogenides CrXTe₃ ($X = \text{Si, Ge}$) belong to a rare class of quasi-two-dimensional semiconducting materials with a ferromagnetic order, band gaps of 0.4 eV for Si and 0.7 eV for Ge compounds, and Curie temperatures (T_C) of 32 and 61 K, respectively [1–6]. Because of their layered structure, due to van der Waals bonding, they can be exfoliated to mono- and few-layer nanosheets, which, together with their semiconducting and magnetic properties, make an ideal combination for applications in optoelectronics and nanospintronics [7–11]. This was further supported by the observation of giant resistivity modulation of CrGeTe₃-based devices [12].

From an x-ray diffraction study [1], it was revealed that CrSiTe₃ crystals are twinned along c axes, the thermal expansion is negative at low temperatures, and the thermal conductivity shows strong magnon-phonon scattering effects. A very small single-ion anisotropy favoring magnetic order along c axes and spin waves was found in CrSiTe₃ by elastic and inelastic neutron scattering [13]. Spin-wave measurements suggest the absence of three-dimensional correlations above T_C , whereas in-plane dynamic correlations are present up to 300 K. First-principles calculations suggested the possibility of graphenelike mechanical exfoliation for CrXTe₃ ($X = \text{Si, Ge}$) single crystals with conserved semiconducting and ferromagnetic properties [14]. The exfoliation of CrSiTe₃ bulk to mono- and few-layer two-dimensional crystals onto a Si/SiO₂ substrate has been achieved [15] with a resistivity between 80 and 120 K, depending on the number of layers. Critical exponents for CrSiTe₃ were also determined from theoretical analysis [16].

Spin-phonon coupling in CrGeTe₃ was investigated in Raman scattering experiments [17]. Splitting of the two lowest-energy E_g modes in the ferromagnetic phase has been observed and ascribed to time-reversal symmetry breaking by

the spin ordering. Furthermore, the significant renormalization of the three higher-energy modes' self-energies below T_C provided additional evidence of spin-phonon coupling [17]. The external pressure-induced effect on lattice dynamics and magnetization in CrGeTe₃ has also been studied [18].

The Raman spectrum of CrSiTe₃ single crystals was reported in Ref. [1], where three Raman-active modes have been observed. Similar results have also been presented in Ref. [15] for ultrathin nanosheets of CrSiTe₃. Here, we report a Raman scattering study of CrSiTe₃ single crystals, with the main focus on phonon properties in the temperature range between 100 and 300 K. Our experimental results are qualitatively different from those previously reported [1,15] but consistent with the results obtained for CrGeTe₃ [17,18]. Furthermore, our data reveal the asymmetry of the E_g^3 mode, which is suppressed at higher temperatures. The A_g^3 and E_g^3 symmetry modes exhibit nonanharmonic self-energy temperature dependence in the region around 180 K, related to the strong spin-lattice interaction due to short-range magnetic order [1]. Energies and symmetries of the observed Raman-active modes are in good agreement with theoretical calculations.

II. EXPERIMENT AND NUMERICAL METHOD

Single crystals of CrSiTe₃ and CrGeTe₃ were grown as described previously [19]. For a Raman scattering experiment, a Tri Vista 557 spectrometer was used in the backscattering micro-Raman configuration with a 1800/1800/2400 grooves/mm diffraction grating combination. A coherent Verdi G solid-state laser with a 532-nm line was used as the excitation source. The direction of the incident (scattered) light coincides with a crystallographic c axis. Right before being placed in the vacuum, the samples were cleaved in the air. All measurements were performed in a high vacuum (10^{-6} mbar) using a KONTI CryoVac continuous-helium-flow cryostat with a 0.5-mm-thick window. Laser-beam focusing was achieved through a microscope objective with $\times 50$ magnification, a spot size of approximately 8 μm , and a power

*nenadl@ipb.ac.rs

TABLE I. Calculated and experimental crystallographic lattice parameters for CrSiTe₃ ($|a| = |b|$), bond lengths, interlayer distance (d), and van der Waals (vdW) gap.

CrSiTe ₃	Calculation (Å)	Experiment (Å) [20]
a	6.87	6.76
c	19.81	20.67
Si-Si	2.27	2.27
Si-Te	2.52	2.51
Cr-Te	2.77	2.78
d	6.86	6.91
vdW gap	3.42	3.42

<2 mW on the surface of a sample. All spectra were corrected for the Bose factor.

Density functional theory calculations were performed in the Quantum Espresso software package [21], using the PBE exchange-correlation functional [22], PAW pseudopotentials [23,24], and energy cutoffs for wave functions and the charge density of 85 and 425 Ry, respectively. For k -point sampling, the Monkhorst-Pack scheme was used, with a Γ -centered $8 \times 8 \times 8$ grid. Optimization of the atomic positions in the unit cell was performed until the interatomic forces were minimized down to 10^{-6} Ry/Å. In order to obtain the parameters accurately, treatment of the van der Waals interactions was included using the Grimme-D2 correction [25]. Phonon frequencies were calculated at the Γ point

TABLE II. (a) Type of atoms, Wyckoff positions, each site's contribution to the phonons at the Γ point, and corresponding Raman tensors for the $R\bar{3}$ space group of CrSiTe₃. (b) Phonon symmetry, calculated optical phonon frequencies at 0 K, and experimental values for Raman-active (at 100 K) and infrared (IR)-active (at 110 K) [1] CrSiTe₃ phonons.

(a) Space group $R\bar{3}$ (No. 148)					
Atom(s) (Wyckoff positions)			Irreducible representations		
Cr, Si (6c)			$A_g + E_g + A_u + E_u$		
Te (18f)			$3A_g + 3E_g + 3A_u + 3E_u$		
(b) Raman tensors					
$A_g = \begin{pmatrix} a & 0 & 0 \\ 0 & b & 0 \\ 0 & 0 & c \end{pmatrix}$		$E_g^1 = \begin{pmatrix} c & d & e \\ d & -c & f \\ e & f & 0 \end{pmatrix}$		$E_g^2 = \begin{pmatrix} d & -c & -f \\ -c & -d & e \\ -f & e & 0 \end{pmatrix}$	
Raman active			IR active [1]		
Symmetry	Calc. (cm ⁻¹)	Expt. (cm ⁻¹)	Symmetry	Calc. (cm ⁻¹)	Expt. (cm ⁻¹)
A_g^1	88.2	–	A_u^1	91.8	91.0
E_g^1	93.5	88.9	E_u^1	93.7	–
E_g^2	96.9	–	A_u^2	116.8	–
E_g^3	118.3	118.2	E_u^2	117.1	–
A_g^2	122.0	–	A_u^3	202.4	–
A_g^3	148.0	147.4	E_u^3	206.2	207.9
A_g^4	208.7	–	A_u^4	243.7	–
E_g^4	219.5	217.2	E_u^4	365.8	370.4
E_g^5	357.4	–			
A_g^5	508.8	–			

within the linear response method implemented in Quantum Espresso. Calculated crystallographic properties obtained by relaxing the structures are in good agreement with x-ray diffraction measurements [20]. A comparison between our, calculated, and experimental results is presented in Table I.

III. RESULTS AND DISCUSSION

A. Polarization dependence

CrSiTe₃ crystallizes in the rhombohedral crystal structure, described by $R\bar{3}$ (C_{3i}^2) [26]. Wyckoff positions of atoms, together with each site's contribution to phonons at the Γ point and corresponding Raman tensors, are listed in Table II. The phonon mode distribution obtained by factor-group analysis for the $R\bar{3}$ space group is as follows:

$$\Gamma_{\text{Raman}} = 5A_g + 5E_g,$$

$$\Gamma_{\text{IR}} = 4A_u + 4E_u,$$

$$\Gamma_{\text{Acoustic}} = A_u + E_u.$$

Since the plane of incidence is ab , where $|a| = |b|$ [$\angle(a, b) = 120^\circ$], and the direction of light propagation is along c axes, from the selection rules, it is possible to observe all Raman-active modes, i.e., five A_g modes and five doubly degenerate E_g modes. According to the Raman tensors presented in Table II, A_g symmetry modes are observable only in the parallel polarization configuration, whereas E_g symmetry

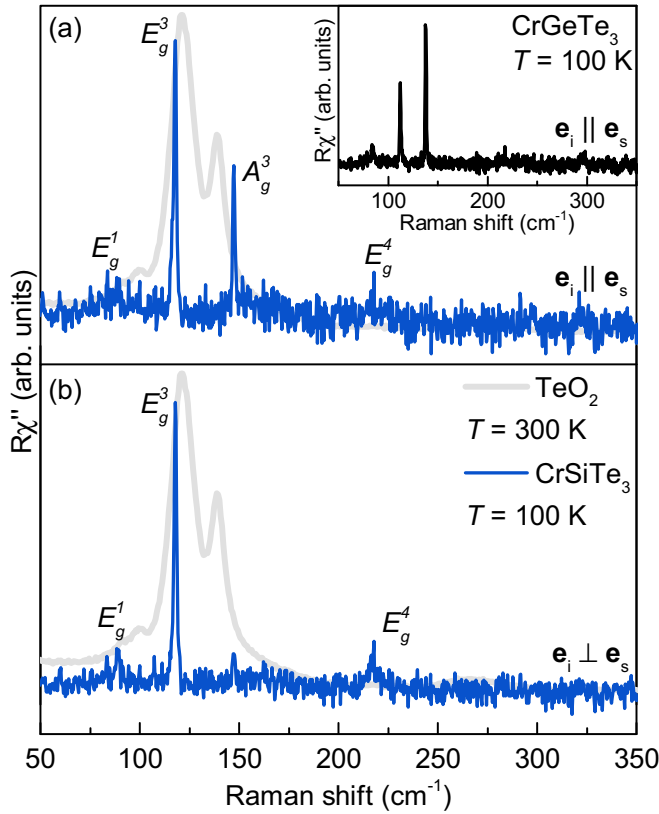


FIG. 1. Raman spectra of CrSiTe₃ single crystals measured at 100 K in (a) parallel and (b) cross polarization configurations. The gray line represents the TeO₂ spectrum measured at 300 K. Inset: Raman spectrum of CrGeTe₃ in the parallel polarization configuration measured at 100 K.

modes can be expected to appear for both in-parallel and cross polarization configurations.

The Raman spectra of CrSiTe₃ for two main linear polarization configurations, at 100 K, are shown in Fig. 1. Four peaks can be observed in the spectra, at energies of 88.9, 118.2, 147.4, and 217.2 cm⁻¹. Since only the peak at 147.4 cm⁻¹ vanishes in the cross polarization configuration, it corresponds to the A_g symmetry mode. The other three modes appear in both parallel and cross polarization configurations and, thereby, can be assigned as E_g symmetry modes (Fig. 1).

In order to exclude the possibility that any of the observed features originate from the TeO₂ [17,27], its Raman spectrum is also presented in Fig. 1. It can be noted that no TeO₂ contribution is present in our CrSiTe₃ data. Furthermore, the observed CrSiTe₃ Raman spectra are also consistent with the CrGeTe₃ Raman spectra (see inset in Fig. 1), isostructural to CrSiTe₃. Five Raman-active modes have been observed for CrGeTe₃, two A_g modes, at 137.9 and 296.6 cm⁻¹, and three E_g modes, at 83.5, 112.2, and 217.5 cm⁻¹, in agreement with the previously published data [17,18]. The main difference in the spectra of CrSiTe₃ and CrGeTe₃ arises from the change in mass and lattice parameter effects that cause the peaks to shift.

Calculated and observed Raman-active phonon energies are compiled in Table II, together with the experimental energies of the infrared (IR)-active phonons [1], and are found to be in good agreement. Displacement patterns of the A_g

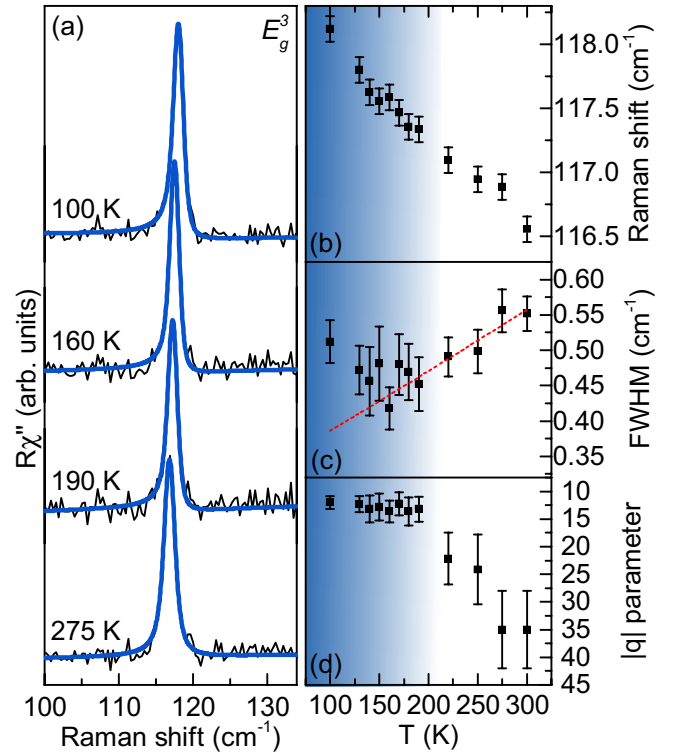


FIG. 2. (a) The E_g³ mode Raman spectra of CrSiTe₃ at four temperatures measured in the cross polarization configuration. Blue lines represent line shapes obtained as a convolution of the Fano line shape and Gaussian, calculated to fit the experimental data. Temperature dependence of (b) the energy, (c) the line width, and (d) the Fano parameter *q* of the E_g³ mode. The dashed red line represents standard anharmonic behavior [28,29]. All the parameters show a change in tendency around 180 K.

and E_g symmetry modes are presented in Fig. 4, in the Appendix.

B. Temperature dependence

After proper assignment of all the observed CrSiTe₃ Raman-active modes we proceeded with temperature evolution of their properties, focusing on the most prominent ones, E_g³ and A_g³. Figure 2(a) shows the spectral region of the doubly degenerate E_g³ mode at an energy of 118.2 cm⁻¹, at four temperatures. Closer inspection of the 100 K spectra revealed clear asymmetry of the peak on the low-energy side. The presence of defects may result in the appearance of the mode asymmetry [30], however, they would also contribute to the mode line width and, possibly, the appearance of phonons from the edge of the Brillouin zone in the Raman spectra [29]. The very narrow lines and absence of additional features in the Raman spectra of CrSiTe₃ do not support this scenario. The asymmetry may also arise when the phonon is coupled to a continuum [31]. Such a coupling of the E_g³ phonon mode would result in a line shape given by the convolution of a Fano function and a Gaussian, the latter representing the resolution of the spectrometer [29]. Comparison between the Fano line shape convoluted with a Gaussian, the Voigt line shape, and the experimental data at 100 K is presented in Fig. 5, in the

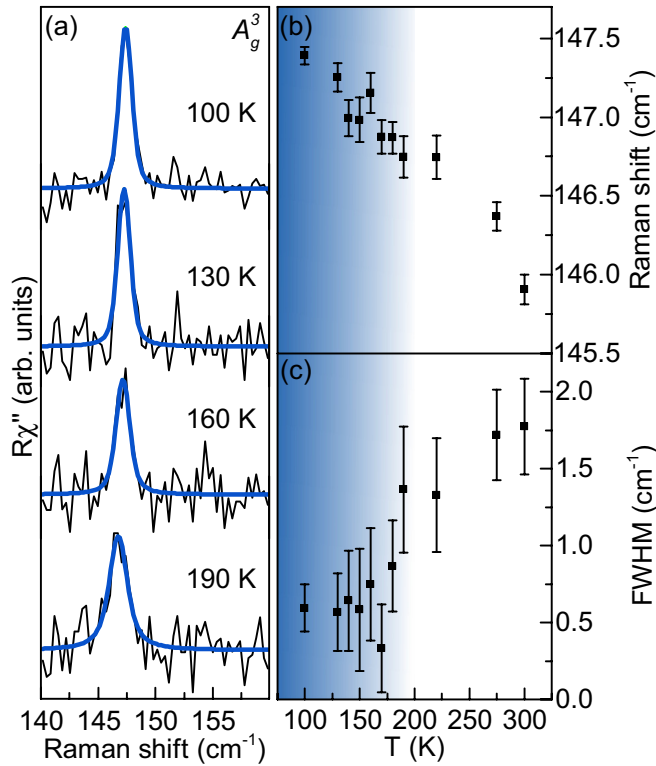


FIG. 3. (a) A_g^3 mode Raman spectra of CrSiTe_3 at four temperatures measured in the parallel polarization configuration. Blue lines represent Voigt line shapes. (b) Energy and (c) line-width temperature dependence of the A_g^3 mode.

Appendix, with the former yielding better agreement with the experimental data. Furthermore, it fully captures the E_g^3 mode line shape at all temperatures under investigation [Figs. 2(a) and 6].

Upon cooling of the sample, the E_g^3 mode energy hardens [Fig. 2(b)] with a very small discontinuity in the temperature range around 180 K. Down to the same temperature, the line width monotonically narrows in line with the standard anharmonic behavior [dashed red line in Fig. 2(c)]. Upon further cooling, the line width increased, deviating from the expected anharmonic tendency. This indicates activation of an additional scattering mechanism, e.g., spin-phonon interaction. Figure 2(d) shows the evolution of the Fano parameter, $|q|$. Whereas in the region below 180 K, it increases slightly but continuously, at higher temperatures it promptly goes to lower values and the mode recovers a symmetric line shape. We believe that the observed behavior of the E_g^3 mode can be traced back to the short-range magnetic correlations, which, according to Ref. [1], persist up to 150 K, and the strong spin-phonon coupling in CrSiTe_3 . Similar behavior of the energy and line width, which differs from the conventional anharmonic, as well as the E_g mode Fano-type line shape, was recently reported in $\alpha\text{-RuCl}_3$ and was interpreted as a consequence of the spin-phonon interaction [32].

Unlike the E_g^3 mode, no pronounced asymmetry was observed for the A_g^3 mode. As can be seen from Figs. 3(b) and 3(c) both the energy and the line width of the A_g^3 mode showed

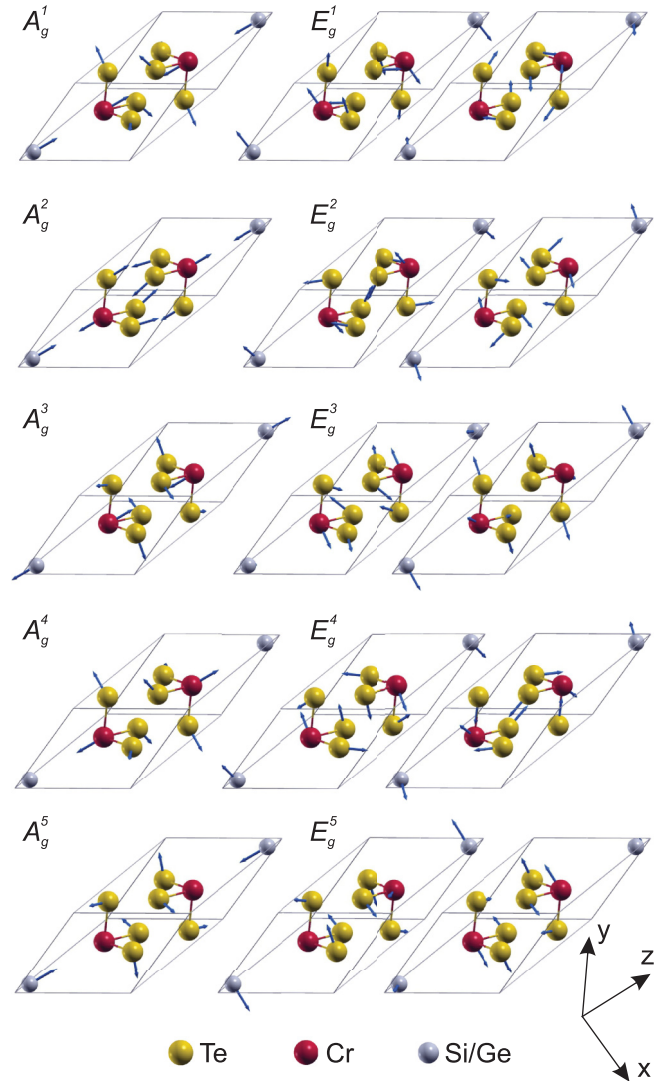


FIG. 4. Unit cell of a CrSiTe_3 single crystal (solid lines) with the displacement patterns of the A_g and E_g symmetry modes. Arrow lengths are proportional to the square root of the interatomic forces.

a similar change in tendency in the same temperature region as the E_g^3 mode, most likely due to the spin-phonon coupling.

IV. CONCLUSION

The lattice dynamics of CrSiTe_3 , a compound isostructural to CrGeTe_3 , is presented. An A_g and three E_g modes were observed and assigned. The experimental results are well supported by theoretical calculations. The temperature dependences of the energies and line widths of the A_g^3 and E_g^3 modes deviate from the conventional anharmonic model in the temperature range around 180 K. In addition, the E_g^3 mode shows clear Fano resonance at lower temperatures. This can be related to the previously reported short-range magnetic correlations at temperatures up to 150 K [1] and the strong spin-phonon coupling.

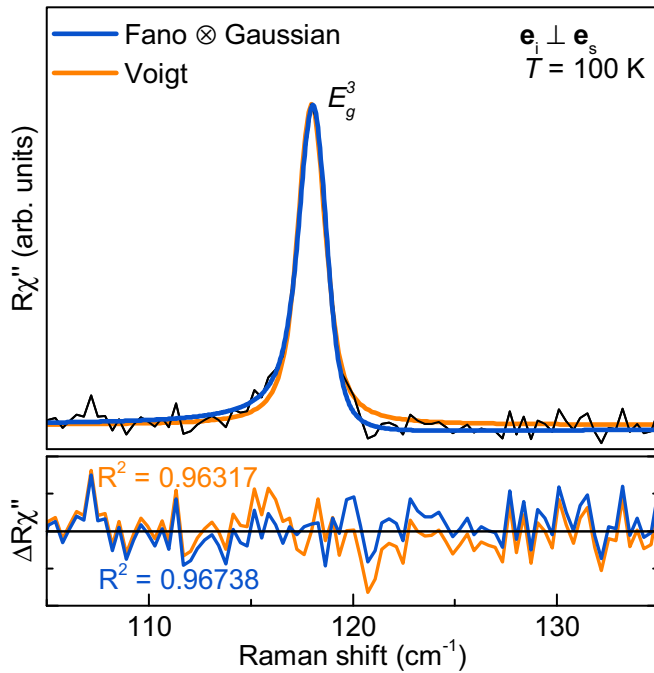


FIG. 5. Analysis of the E_g^3 asymmetry. Measured data are shown as the black line. The solid blue line represents the line shape obtained as a convolution of the Fano line shape and a Gaussian, whereas the orange line represents a Voigt line shape, both calculated to fit the experimental data. The Voigt profile deviates from the experimental data at the peak flanks.

ACKNOWLEDGMENTS

The work was supported by the Serbian Ministry of Education, Science and Technological Development under Projects III45018 and OI171005. DFT calculations were performed using computational resources at Johannes Kepler University, Linz, Austria. Work at Brookhaven was supported by the US Department of Energy, Office of Basic Energy Sciences as part of the Computation Material Science Program (material synthesis and characterization).

A.M. and N.L. conceived and performed the experiment, analyzed and discussed data, and wrote the paper; A.S. and J.P. calculated phonon energies, analyzed and discussed data, and wrote the paper; Y.L. and C.P. synthesized and characterized the samples; Z.V.P. analyzed and discussed data and wrote the paper. All authors commented on the manuscript.

APPENDIX

1. Eigenvectors of Raman-active modes

Figure 4 summarizes the A_g and E_g symmetry mode displacement patterns of a CrSiTe₃ single crystal ($R\bar{3}$ space group). Arrow lengths are proportional to the square root of the interatomic forces.

2. Asymmetry of the E_g^3 line

The peak at 118.2 cm^{-1} , which we assigned as the E_g^3 symmetry mode, at low temperatures shows a significant asymmetry towards lower energies. The possibility of additional

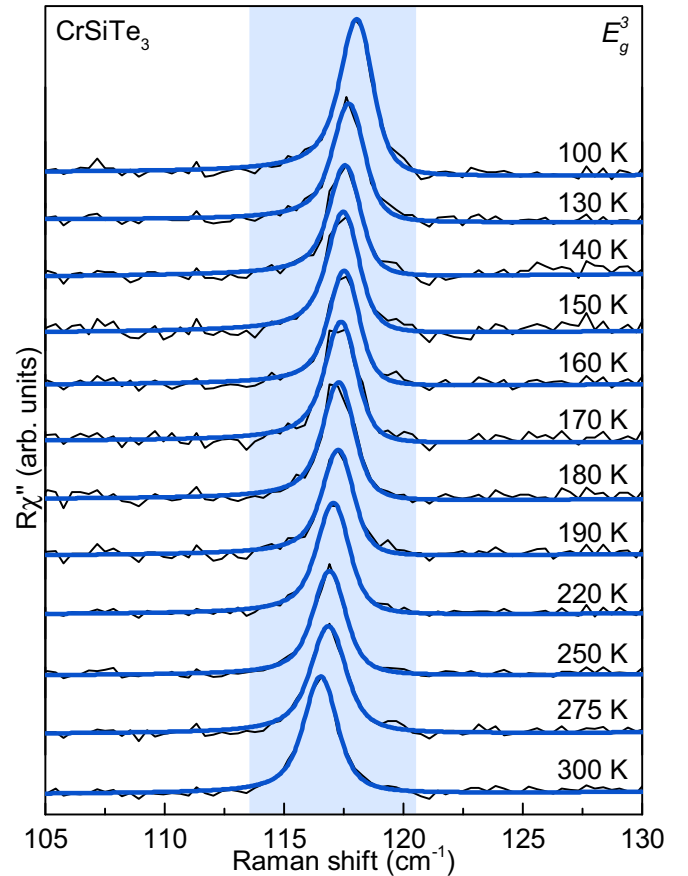


FIG. 6. The E_g^3 mode Raman spectra of CrSiTe₃ at all temperatures measured in the cross polarization configuration. Blue lines represent calculated spectra obtained as the convolution of the Fano line shape and Gaussian.

defect-induced features in Raman spectra can be excluded, since the modes are very narrow, suggesting high crystallinity of the sample. Also, the theoretical calculations do not predict additional Raman-active modes in this energy region. On the other hand, coupling of the phonon mode to a continuum may result in an asymmetric line shape described with the Fano function. Due to the finite resolution of the spectrometer it has to be convoluted with a Gaussian ($\Gamma_G = 1 \text{ cm}^{-1}$). In Fig. 5 we present a comparison of the line obtained as a convolution of the Fano line shape and a Gaussian (blue line) and a Voigt line shape (orange line) fitted to the experimental data. Whereas the Voigt line shape deviates at the peak flanks, excellent agreement has been achieved for convolution of the Fano line shape and a Gaussian.

3. E_g^3 mode temperature dependence

Figure 6 shows Raman spectra of CrSiTe₃ in the region of the E_g^3 mode in the cross polarization configuration at various temperatures. Solid blue lines represent the convolution of the Fano line shape and Gaussian fitted to the experimental data. The asymmetry is the most pronounced below 190 K. Above this temperature, the asymmetry is decreasing, and at high temperatures the peak recovers the fully symmetric line shape.

- [1] L. D. Casto, A. J. Clune, M. O. Yokosuk, J. L. Musfeldt, T. J. Williams, H. L. Zhuang, M.-W. Lin, K. Xiao, R. G. Hennig, B. C. Sales, J.-Q. Yan, and D. Mandrus, Strong spin-lattice coupling in CrSiTe₃, *APL Mater.* **3**, 041515 (2015).
- [2] X. Zhang, Y. Zhao, Q. Song, S. Jia, J. Shi, and W. Han, Magnetic anisotropy of the single-crystalline ferromagnetic insulator Cr₂Ge₂Te₆, *Jpn. J. Appl. Phys.* **55**, 033001 (2016).
- [3] T. Leineweber and H. Kronmüller, Micromagnetic examination of exchange coupled ferromagnetic nanolayers, *J. Magn. Magn. Mater.* **176**, 145 (1997).
- [4] G. Ouvrard, E. Sandre, and R. Brec, Synthesis and crystal structure of a new layered phase: The chromium hexatellurosilicate Cr₂Si₂Te₆, *J. Solid State Chem.* **73**, 27 (1988).
- [5] B. Siberchicot, S. Jobic, V. Carreaux, P. Gressier, and G. Ouvrard, Band structure calculations of ferromagnetic chromium tellurides CrSiTe₃ and CrGeTe₃, *J. Phys. Chem.* **100**, 5863 (1996).
- [6] V. Carreaux, F. Moussa, and M. Spiesser, 2D Ising-like ferromagnetic behaviour for the lamellar Cr₂Si₂Te₆ compound: A neutron scattering investigation, *Europhys. Lett.* **29**, 251 (1995).
- [7] N. Sivasdas, M. W. Daniels, R. H. Swendsen, S. Okamoto, and D. Xiao, Magnetic ground state of semiconducting transition-metal trichalcogenide monolayers, *Phys. Rev. B* **91**, 235425 (2015).
- [8] K. S. Novoselov, A. K. Geim, S. V. Morozov, D. Jiang, Y. Zhang, S. V. Dubonos, I. V. Grigorieva, and A. A. Firsov, Electric field effect in atomically thin carbon films, *Science* **306**, 666 (2004).
- [9] Q. H. Wang, K. Kalantar-Zadeh, A. Kis, J. N. Coleman, and M. S. Strano, Electronics and optoelectronics of two-dimensional transition metal dichalcogenides, *Nat. Nanotechnol.* **7**, 699 (2012), review Article.
- [10] C. Gong, L. Li, Z. Li, H. Ji, A. Stern, Y. Xia, T. Cao, W. Bao, C. Wang, Y. Wang, Z. Q. Qiu, R. J. Cava, S. G. Louie, J. Xia, and X. Zhang, Discovery of intrinsic ferromagnetism in two-dimensional van der Waals crystals, *Nature* **546**, 265 (2017).
- [11] B. Huang, G. Clark, E. Navarro-Moratalla, D. R. Klein, R. Cheng, K. L. Seyler, D. Zhong, E. Schmidgall, M. A. McGuire, D. H. Cobden, W. Yao, D. Xiao, P. Jarillo-Herrero, and X. Xu, Layer-dependent ferromagnetism in a van der Waals crystal down to the monolayer limit, *Nature* **546**, 270 (2017).
- [12] W. Xing, Y. Chen, P. M. Odenthal, X. Zhang, W. Yuan, T. Su, Q. Song, T. Wang, J. Zhong, S. Jia, X. C. Xie, Y. Li, and W. Han, Electric field effect in multilayer Cr₂Ge₂Te₆: A ferromagnetic 2D material, *2D Mater.* **4**, 024009 (2017).
- [13] T. J. Williams, A. A. Aczel, M. D. Lumsden, S. E. Nagler, M. B. Stone, J.-Q. Yan, and D. Mandrus, Magnetic correlations in the quasi-two-dimensional semiconducting ferromagnet CrSiTe₃, *Phys. Rev. B* **92**, 144404 (2015).
- [14] X. Li and J. Yang, CrXTe₃ (X = Si, Ge) nanosheets: Two dimensional intrinsic ferromagnetic semiconductors, *J. Mater. Chem. C* **2**, 7071 (2014).
- [15] M.-W. Lin, H. L. Zhuang, J. Yan, T. Z. Ward, A. A. Puretzy, C. M. Rouleau, Z. Gai, L. Liang, V. Meunier, B. G. Sumpter, P. Ganesh, P. R. C. Kent, D. B. Geohegan, D. G. Mandrus, and K. Xiao, Ultrathin nanosheets of CrSiTe₃: A semiconducting two-dimensional ferromagnetic material, *J. Mater. Chem. C* **4**, 315 (2016).
- [16] B. Liu, Y. Zou, S. Zhou, L. Zhang, Z. Wang, H. Li, Z. Qu, and Y. Zhang, Critical behavior of the van der Waals bonded high T_C ferromagnet Fe₃GeTe₂, *Sci. Rep.* **7**, 6184 (2017).
- [17] Y. Tian, M. J. Gray, H. Ji, R. J. Cava, and K. S. Burch, Magneto-elastic coupling in a potential ferromagnetic 2D atomic crystal, *2D Mater.* **3**, 025035 (2016).
- [18] Y. Sun, R. C. Xiao, G. T. Lin, R. R. Zhang, L. S. Ling, Z. W. Ma, X. Luo, W. J. Lu, Y. P. Sun, and Z. G. Sheng, Effects of hydrostatic pressure on spin-lattice coupling in two-dimensional ferromagnetic Cr₂Ge₂Te₆, *Appl. Phys. Lett.* **112**, 072409 (2018).
- [19] Y. Liu and C. Petrovic, Critical behavior of quasi-two-dimensional semiconducting ferromagnet Cr₂Ge₂Te₆, *Phys. Rev. B* **96**, 054406 (2017).
- [20] G. T. Lin, H. L. Zhuang, X. Luo, B. J. Liu, F. C. Chen, J. Yan, Y. Sun, J. Zhou, W. J. Lu, P. Tong, Z. G. Sheng, Z. Qu, W. H. Song, X. B. Zhu, and Y. P. Sun, Tricritical behavior of the two-dimensional intrinsically ferromagnetic semiconductor CrGeTe₃, *Phys. Rev. B* **95**, 245212 (2017).
- [21] P. Giannozzi, S. Baroni, N. Bonini, M. Calandra, R. Car, C. Cavazzoni, D. Ceresoli, G. L. Chiarotti, M. Cococcioni, I. Dabo, A. D. Corso, S. de Gironcoli, S. Fabris, G. Fratesi, R. Gebauer, U. Gerstmann, C. Gougoussis, A. Kokalj, M. Lazzeri, L. Martin-Samos, N. Marzari, F. Mauri, R. Mazzarello, S. Paolini, A. Pasquarello, L. Paulatto, C. Sbraccia, S. Scandolo, G. Sclauzero, A. P. Seitsonen, A. Smogunov, P. Umari, and R. M. Wentzcovitch, Quantum espresso: A modular and open-source software project for quantum simulations of materials, *J. Phys.: Condens. Matter* **21**, 395502 (2009).
- [22] J. P. Perdew, K. Burke, and M. Ernzerhof, Generalized Gradient Approximation Made Simple, *Phys. Rev. Lett.* **77**, 3865 (1996).
- [23] P. E. Blöchl, Projector augmented-wave method, *Phys. Rev. B* **50**, 17953 (1994).
- [24] G. Kresse and D. Joubert, From ultrasoft pseudopotentials to the projector augmented-wave method, *Phys. Rev. B* **59**, 1758 (1999).
- [25] G. Stefan, Semiempirical GGA-type density functional constructed with a long-range dispersion correction, *J. Comput. Chem.* **27**, 1787 (2006).
- [26] R. E. Marsh, The crystal structure of Cr₂Si₂Te₆: Corrigendum, *J. Solid State Chem.* **77**, 190 (1988).
- [27] N. Lazarević, E. S. Bozin, M. Šćepanović, M. Opačić, Hechang Lei, C. Petrovic, and Z. V. Popović, Probing IrTe₂ crystal symmetry by polarized Raman scattering, *Phys. Rev. B* **89**, 224301 (2014).
- [28] M. Opačić, N. Lazarević, M. Šćepanović, H. Ryu, H. Lei, C. Petrovic, and Z. V. Popović, Evidence of superconductivity-induced phonon spectra renormalization in alkali-doped iron selenides, *J. Phys.: Condens. Matter* **27**, 485701 (2015).
- [29] A. Baum, A. Milosavljević, N. Lazarević, M. M. Radonjić, B. Nikolić, M. Mitschek, Z. Inanloo Maranloo, M. Šćepanović, M. Grujić-Brojčin, N. Stojilović, M. Opel, Aifeng Wang, C. Petrovic, Z. V. Popović, and R. Hackl, Phonon anomalies in FeS, *Phys. Rev. B* **97**, 054306 (2018).

- [30] N. Lazarević, M. Radonjić, M. Šćepanović, Hechang Lei, D. Tanasković, C. Petrovic, and Z. V. Popović, Lattice dynamics of KNi₂Se₂, *Phys. Rev. B* **87**, 144305 (2013).
- [31] N. Lazarević, Z. V. Popović, Rongwei Hu, and C. Petrovic, Evidence for electron-phonon interaction in Fe_{1-x}M_xSb₂ ($M = \text{Co}$ and Cr ; $0 \leq x \leq 0.5$) single crystals, *Phys. Rev. B* **81**, 144302 (2010).
- [32] L. J. Sandilands, Y. Tian, K. W. Plumb, Y.-J. Kim, and K. S. Burch, Scattering Continuum and Possible Fractionalized Excitations in α -RuCl₃, *Phys. Rev. Lett.* **114**, 147201 (2015).

Correction: Missing support information in the Acknowledgment section has been inserted.